ORIGINAL ARTICLE

JBMR®

Suppression of Sost/Sclerostin and Dickkopf-1 Augment Intervertebral Disc Structure in Mice

Tori Kroon,[1] Neharika Bhadouria,[2] Paul Niziolek,[3] Daniel Edwards III,[4] Roy Choi,[5] Erica L Clinkenbeard,[4] Alexander Robling,[4,5] and Nilsson Holguin[4,5,6]

[1]Department of Biomedical Engineering, IUPUI, Indianapolis, IN, USA
[2]Department of Mechanical Engineering, Purdue University, West Lafayette, IN, USA
[3]Radiology & Imaging Sciences, IUPUI, Indianapolis, IN, USA
[4]Indiana Center of Musculoskeletal Health, Indianapolis, IN, USA
[5]Department for Anatomy and Cell Biology, IUPUI, Indianapolis, IN, USA
[6]Department of Mechanical and Energy Engineering, IUPUI, Indianapolis, IN, USA

ABSTRACT

Intervertebral disc (IVD) degeneration is a leading cause of low back pain, characterized by accelerated extracellular matrix breakdown and IVD height loss, but there is no approved pharmacological therapeutic. Deletion of Wnt ligand competitor Lrp5 induces IVD degeneration, suggesting that Wnt signaling is essential for IVD homeostasis. Therefore, the IVD may respond to neutralization of Wnt ligand competitors *sost*(gene)/sclerostin(protein) and/or dickkopf-1 (dkk1). Anti-sclerostin antibody (scl-Ab) is an FDA-approved bone therapeutic that activates Wnt signaling. We aimed to (i) determine if pharmacological neutralization of sclerostin, dkk1, or their combination would stimulate Wnt signaling and augment IVD structure and (ii) determine the prolonged adaptation of the IVD to global, persistent deletion of *sost*. Nine-week-old C57Bl/6J female mice ($n = 6$–7/group) were subcutaneously injected 2×/week for 5.5 weeks with scl-Ab (25 mg/kg), dkk1-Ab (25 mg/kg), 3:1 scl-Ab/dkk1-Ab (18.75:6.25 mg/kg), or vehicle (veh). Separately, IVD of *sost* KO and wild-type (WT) mice ($n = 8$/group) were harvested at 16 weeks of age. First, compared with vehicle, injection of scl-Ab, dkk1-Ab, and 3:1 scl-Ab/dkk1-Ab similarly increased lumbar IVD height and β-catenin gene expression. Despite these similarities, only injection of scl-Ab alone strengthened IVD mechanical properties and decreased heat shock protein gene expressions. Genetically and compared with WT, *sost* KO enlarged IVD height, increased proteoglycan staining, and imbibed IVD hydration. Notably, persistent deletion of *sost* was compensated by upregulation of *dkk1*, which consequently reduced the cell nuclear fraction for Wnt signaling co-transcription factor β-catenin in the IVD. Lastly, RNA-sequencing pathway analysis confirmed the compensatory suppression of Wnt signaling and revealed a reduction of cellular stress-related pathways. Together, suppression of sost/sclerostin or dkk1 each augmented IVD structure by stimulating Wnt signaling, but scl-Ab outperformed dkk1-Ab in strengthening the IVD. Ultimately, postmenopausal women prescribed scl-Ab injections to prevent vertebral fracture may also benefit from a restoration of IVD height and health. © 2022 The Authors. *Journal of Bone and Mineral Research* published by Wiley Periodicals LLC on behalf of American Society for Bone and Mineral Research (ASBMR).

KEY WORDS: ANABOLIC THERAPEUTICS; CHONDROCYTE AND CARTILAGE BIOLOGY; GENETIC ANIMAL MODELS; PRECLINICAL STUDIES; WNT/β-CATENIN/LRPs

Introduction

There are no FDA-approved pharmacological treatments for intervertebral disc (IVD) degeneration,[1,2] a major contributing factor of low back pain.[3,4] Osteoporosis may contribute to IVD degeneration[5] and some pharmacological treatments for bone maintenance target anabolic pathways innate to the IVD. Anti-sclerostin-antibody (scl-Ab) treatment is an FDA-approved bone anabolic[6] for postmenopausal women at high risk of vertebral fracture.[7] Sclerostin and dkk1 are inhibitors of the Wnt/β-catenin signaling pathway and global suppression of sclerostin by systemic injection of scl-Ab or genetic ablation of its precursor *SOST(human)/sost(mouse)* promotes bone formation and mildly attenuates bone resorption.[8] Individuals administered scl-Ab

Received in original form July 9, 2021; revised form March 2, 2022; accepted March 10, 2022.
Address correspondence to: Nilsson Holguin, PhD, Department of Orthopaedics, Icahn School of Medicine at Mount Sinai, 1268 Madison Ave, New York, NY 10025, USA. E-mail: nilsson.holguin@mssm.edu
Additional Supporting Information may be found in the online version of this article.
Journal of Bone and Mineral Research, Vol. 37, No. 6, June 2022, pp 1156–1169.
DOI: 10.1002/jbmr.4546

do not report an altered incidence of back pain than control subjects, suggesting it might not be harmful to the IVD.[6] Although osteocytes in bone are the major source of sclerostin[9,10] and dickkopf-1 (dkk1),[11] IVD cells also express sclerostin and dkk1,[12] but the impact of regulating sost/sclerostin or dkk1 on the IVD has yet to be determined.

Sclerostin and dkk1 are inhibitors of the canonical Wnt signaling pathway but differ in some notable ways. Both dkk1 and sclerostin interact with LRP5/6 to competitively prevent various Wnt ligands from binding to initiate the canonical Wnt signaling pathway.[11] β-catenin is a key co-transcription factor in the Wnt signaling pathway, where activation of this pathway is composed of β-catenin translocation to the cell nucleus, association with co-transcription factors T-cell factor (TCF) and lymphoid enhancer factor (LEF), and transcription of target genes.[13] Wnt/β-catenin signaling regulates cell fate and extracellular matrix (ECM) anabolism in a range of musculoskeletal tissues. For instance, inactivation of Wnt signaling shifts differentiation of mesenchymal stem cells from osteoblastogenesis to chondrogenesis[14] and activation in early chondrocytes triggers hyperchondrocyte maturation.[15] Sclerostin and dkk1 can both bind to the first β-propeller of LRP5/6, but dkk1 can also bind to the second, third, and fourth β-propellers of LRP5/6.[16-18] A pathway-related distinction between dkk1 and sclerostin is that dkk1 is a direct target of Wnt/β-catenin signaling pathway.[19]

In the spine, IVD development requires Wnt signaling,[20] and loss of Wnt signaling by aging and/or injury[21,22] blunts ECM anabolism.[12,21] The nucleus pulposus serves as the hydration core of the IVD and houses notochordal cells that require Wnt signaling to maintain their cellular phenotype.[23] Age- and injury-related reduction of Wnt signaling trigger the replacement of notochordal cells by more mature nucleus pulposus cells that are less equipped to produce ECM.[21,24] Contrarily, genetic stabilization of β-catenin in the nucleus pulposus increases notochordal cell expression and ECM anabolism[24] and can promote ECM-related transcription during IVD injury.[12] Lastly, in vivo deletion of LRP5 in IVD cells reduces Wnt signaling[21] and suggests that the IVD may be sensitive to Wnt ligand competitors that bind LRP5/6.

Therefore, we hypothesized that (i) neutralization of sclerostin and/or dkk1 and (ii) deletion of gene precursor to sclerostin *sost* would stimulate ECM anabolism in the IVD by increasing canonical Wnt signaling. Neutralization of sclerostin, dkk1, and in combination similarly increased Wnt signaling and IVD height. Next, using histology, MRI, qPCR, and RNA sequencing, global genetic deletion of *sost* increased the water content of the IVD, proteoglycan staining, IVD height, and decreased cellular stress mechanisms related to protein folding, but these changes were accompanied by gene and protein expression changes consistent with mature cell phenotypes by compensation of Wnt signaling. Overall, suppression of *sost*/sclerostin and/or dkk1 augment the structure of the IVD.

Materials and Methods

Mice

Nine-week-old C57Bl/6J female mice (n = 6–7/group) were injected with 25 mg/kg of either anti-sclerostin antibody (scl-Ab), anti-dkk1 antibody (dkk1-Ab), a 3:1 ratio of the two antibodies (18.75 mg/kg of scl-Ab and 6.25 mg/kg of dkk1-Ab), a 1:1 ratio (12.5 mg/kg of scl-Ab and dkk1-Ab), a 1:3 ratio (6.25 mg/kg of scl-Ab and 18.75 mg/kg of dkk1-Ab), or the buffer in which the antibodies were made (veh) for 5.5 weeks, twice per week (all previously described;[25,26] Table 1). L3–S1 of these mice were used for another study and not analyzed here. *Sost* KO mice and their wild-type (WT) littermates (n = 8/group total) on a C57Bl/6 background have been previously described.[25] Mice were housed in a 12-hour light/dark cycle, fed standard chow, and all experiments were performed with prior IACUC approval. Lumbar and caudal (tail) spinal sections were harvested. Mice were euthanized by hypoxia as a primary means and cervical dislocation as a secondary means. Spinal levels were further divvied-up for specific testing (Table 2).

Histology and immunohistochemistry

IVD for each stain were run in a single batch. L1–3 and CC10–11 were fixed in 15 mL of 10% formalin on a rocker for 24 hours, submerged in 70% ethanol, embedded in paraffin, and sectioned (5 μm). Safranin O/fast green counterstain images were analyzed by four independent observers for an average IVD degeneration score.[21,27] In short, the nucleus pulposus (NP), annulus fibrosus (AF), and boundary between the two structures were scored based on structural properties and added for a total IVD score between 0 and 14, with increasing scores denoting greater IVD degeneration. Qualitatively, proteoglycan in the NP was estimated as the amount of intensity staining per area using ImageJ. Alcian blue staining was the counterstain for the IHC staining of sclerostin (BAF 1589, R&D Systems, Minneapolis, MN, USA), osterix (#22552, Abcam, Cambridge, MA, USA), and collagen 2 (II-II6B3-c, DSHB, Iowa City, IA, USA). For both osterix and collagen 2 quantification in the NP, positive cells were counted and compared with the total number of cells that were stained brown for the protein and blue for the cell nuclei. The percent of the area-stained brown for osterix was quantified and compared for the AF. Samples with sectioning anomalies and statistical outliers (see Statistics) were excluded from analysis. Total sample size per group was noted in each figure description.

Mechanical testing and analysis

After extraction of CC6–CC7 motion segments, the IVD was prepared, mechanically tested, and analyzed based on a previously published technique.[28] The IVD was isolated from vertebrae CC6 and CC7 by dissection at the growth plate with the assistance of a microscope (M400 Photomakroscop; Wild, Heerbrugg, Switzerland). Growth plate-IVD-growth plate segments were imaged by an X-ray machine (Bruker, Kontich, Belgium) to determine IVD height using ImageJ (NIH). Next, a petri dish was glued to each IVD using cyanoacrylate and filled with phosphate buffered saline (PBS, pH 7.2) to maintain an osmotic environment. IVD were tested using a microindentation system (BioDent;

Table 1. Scl-Ab and/or Dkk1-Ab Dosage

Group	Scl-Ab (mg/kg)	Dkk1-Ab (mg/kg)	Total Ab (mg/kg)	*n*
Veh	0	0	0	7
Scl-Ab	25	0	25	6
Dkk1-Ab	0	25	25	7
3:1	18.75	6.25	25	7
1:1	12.5	12.5	25	7
1:3	6.25	18.75	25	7

Table 2. Functional Spinal Unit or Bone for Each Outcome

Outcome	Tail	Lumbar
MRI	CC6–7	N/A
Mechanics	CC6–7	N/A
Western blot	CC6–8, CC10–12	N/A
μCT	CC7	L6
qPCR	CC8–10, CC4–5, and CC14–15	L3–5
Histology	CC11–13	L1–3

N/A = not applicable. CC4–5 and CC14–15 segments used for the injection-related groups.

Active Life Scientific, Santa Barbara, CA, USA) for quasi-static and dynamic mechanical properties. The testing sample was aligned with a 2.39 mm probe that fully covered the entire IVD and loaded sinusoidally (1 Hz) for 20 cycles under a preload of 20 grams at a compressive strain of 5%. Compressive strains were determined using X-ray-derived IVD heights. Triplicate trials were performed at each strain, with at least 10 minutes of rest time between each trial.

MATLAB code was used to remove the noise generated from the first and last loading cycle in the force-distance curve for each trial. The mechanical property outcomes from a semi-automated software program included relative maximum force (N), displacement (μm), loading stiffness (N/μm), unloading stiffness (N/μm), energy dissipation (N·μm = μJ), and loss tangent from the force-distance curve. Relative maximum force and displacement were calculated by considering the difference between the maximum and minimum values for these outcomes. Each outcome was computed as the average of the two trials with the lowest standard deviation out of three trials.

Magnetic resonance imaging (MRI)

Motion segment CC6–7 was submerged and wrapped in 1× PBS-soaked gauze overnight until imaged. Imaging was completed on the Bruker BioSpin 9.4 T MRI, using a 400-nm-slice thickness for 2D imaging. The motion segment was imaged in a sagittal orientation using a 0.052 × 0.052 mm voxel resolution in the *x*–*y* direction and a 0.4 mm voxel resolution in the *z* direction taking 16 averages/slice. Two samples were stacked in a glass tube to remain upright, and two glass tubes were placed, separated by foam composite, inside of a 15 mL tube to ensure samples would not move while being imaged. Images were analyzed for quantification by ImageJ (NIH). Area and intensity of the IVD were determined and multiplied to estimate the hydration content of the IVD.

Micro-computed tomography

Motion segments L6–S1 and CC6–7 were harvested and submerged in 1× PBS before imaging. Specimens were imaged using the Bruker SkyScan 1272 Micro-CT at a resolution of 8 μm. Vertebral bone was contoured at the periosteum and endosteum for trabecular and cortical analysis. For the trabecular analysis, the growth plate was used as a landmark and trabecular bone analysis consisted of the next 30 consecutive images (slices).[29] For cortical analysis, the longitudinal center of the bone was identified and 15 images above and below were analyzed using the Bruker CTan64 MicroCT software.[17] Parameters measured included bone volume/tissue volume (BV/TV), trabecular number (Tb.N), trabecular thickness (Tb.Th) for trabecular bone, and cross-sectional thickness for cortical bone, using a lower threshold of 60 and upper threshold of 225 for analysis.

QPCR

L3–5 and CC8-10 IVDs were harvested, frozen in liquid nitrogen, pulverized, and suspended in TRIZOL (Ambion, Austin, TX, USA) until further processing.[17] RNA isolation and purification steps were followed (RNeasy Mini Kit, Qaigen, Valencia, CA, USA) and RNA concentration was quantified (Nanodrop, Thermo Fisher Scientific, Waltham, MA, USA). CDNA was synthesized (iScript, Bio-Rad, Hercules, CA, USA) from 400 ng of total RNA for the following Taqman probes (Life Technologies, Carlsbad, CA, USA); *aggrecan* (Mm00565794_m1), *keratin8* (Mm04209403_g1), *dmp1* (Mm01208363_m1), *sost* (Mm00470479_m1), *adamts5* (Mm00478620_m1), *collagen1* (Mm00801666_g1), *collagen2* (Mm01309565_m1), *osterix* (Mm04209856_m1), *β-catenin* (Mm01350387_g1), *serpina1a* (Mm02748447_g1), *serpina1c*+(Mm04207703_mH), *serpina1d* (Mm00842095_mH), *sostdc1* (Mm03024258_s1), *foxa2* (Mm01976556_s1), *axin2* (Mm00443610_m1), *sfrp4* (Mm00840104_m1), *gdf5* (Mm00433564_m), *hspa1b* (Mm03038954_s1), *cxcl9* (Mm00434946_m1), *il1b* (Mm00434228_m1), *wnt16* (Mm00446420_m1), *dkk1* (Mm00438422_m1), *Wnt3a* (Mm00437337_m1). Relative gene expression was normalized to *IPO8* (Mm01255158_m1) for each group and then experimental values (*sost* KO) were normalized to the average of the WT values ($2^{-\Delta\Delta CT}$).

Western blotting

WT and *sost* KO IVDs between CC6–8 were isolated for whole-cell lysate and cytoplasmic and nuclear separation Western blots.[30] IVDs were minced in ice-cold PBS (Thermo Fisher) containing 2% fetal bovine serum (FBS; Atlanta Biologicals, Flowery Branch, GA, USA) and protease inhibitor PMSF (Sigma, St. Louis, MO, USA). Two-tail IVDs from a single animal, per isolation method, were homogenized using a Tissue Tearor (BioSpec Products, Bartlesville, OK, USA). Whole-cell lysate was generated using diluted 1× cell lysis buffer (Cell Signaling, Danvers, MA, USA) supplemented with PMSF. Fractionation of the nuclear protein was performed according to the Pierce cytoplasmic and nuclear extraction kit instructions (Sigma). Samples were run on an SDS-Page gel (Bio-Rad) and transferred to PVDF membrane (Bio-Rad). Blots were probed for anti-β-catenin (unphosphorylated; Cell Signaling) and subsequently an HRP-tagged anti-rabbit secondary antibody (#7074S, Cell Signaling). Whole-cell lysates were normalized to HRP-tagged actin antibody (#A3854, Sigma-Aldrich) and nuclear fractions to HRP-tagged histone H3 (#12648, Cell Signaling). All blots were developed using Immobilon Luminata Forte (Sigma), and the images were digitally collected with the Amersham Imager 600 (GE Healthcare, Madison, WI, USA). Densitometry quantification was conducted on ImageJ to enumerate relative protein values between groups.

Bioinformatics

Gene set enrichment analysis (GSEA) software was used to generate the top down- and upregulated pathways by deletion of *sost* in the IVD. The input included gene name and raw counts for each sample. WEB-based Gene SeT AnaLysis Toolkit was used

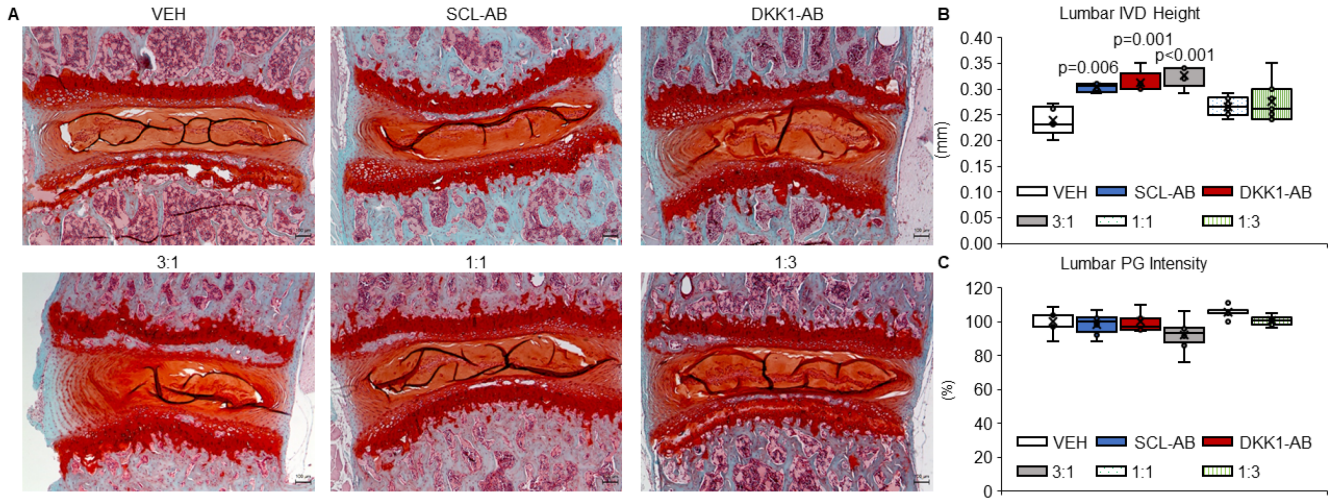

Fig. 1. Quantitative and qualitative intervertebral disc (IVD) structural properties. (*A*) Magnified images (5×) of Safranin O and fast green counterstained histological sections of the lumbar IVD for vehicle (veh, $n = 5$ mice), 25 mg/kg anti-sclerostin-antibody injection (scl-Ab, $n = 5$), and25 mg/kg injection of anti-dkk1-antibody (dkk1-Ab, $n = 5$) (top row, left to right) and combination injection of 18.75 mg/kg anti-sclerostin-antibody and 6.25 mg/kg anti-dkk1-antibody (3:1, $n = 5$), combination of 12.5 mg/kg each of anti-sclerostin- and anti-dkk1-antibody (1:1, $n = 7$), and a combination injection of 6.25 mg/kg of anti-sclerostin-antibody and 18.75 mg/kg of anti-dkk1-antibody (1:3, $n = 6$) (bottom row, left to right). (*B*) Quantitative measurement of lumbar IVD height of all 6 groups. (*C*) Quantitative measurement of proteoglycan intensity staining in percentage of the lumbar IVD. Red staining for proteoglycan. Scale bar = 100 μm. Injection groups were compared with the vehicle group using a Dunnett's test, with significance noted below $p < 0.05$.

to generate the top up- and downregulated pathways between the WT and *sost* KO group. Using GSEA method of interest and geneontology for the functional database, the input included gene symbols and associated fold change for each gene. R Studio was used to generate plots such as PCA plot, volcano plot, and heat maps.

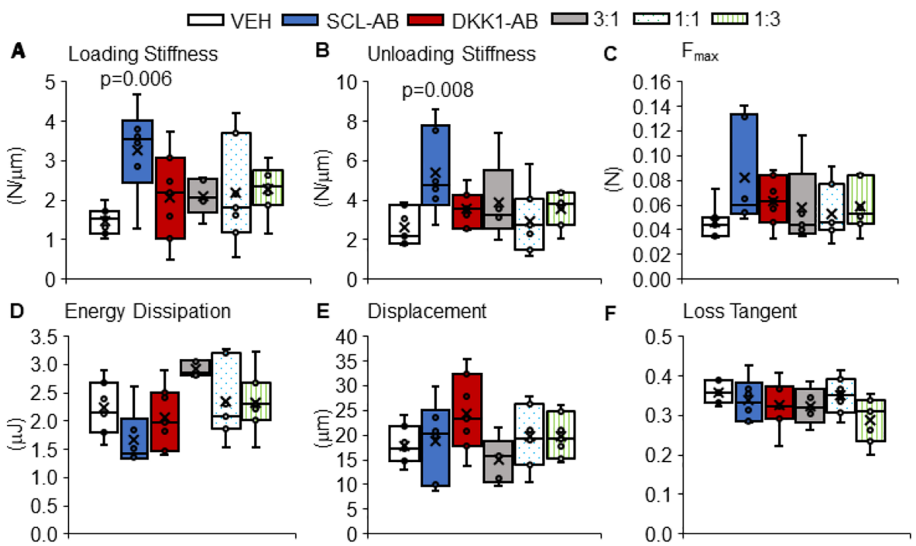

Fig. 2. Injection of Scl-Ab improved intervertebral disc (IVD) mechanical properties. C57Bl6 mice were injected with vehicle (veh, $n = 7$ mice), 25 mg/kg anti-sclerostin-antibody injection (scl-Ab, $n = 6$), 25 mg/kg injection of anti-dkk1-antibody (dkk1-Ab, $n = 7$), combination injection of 18.75 mg/kg anti-sclerostin-antibody and 6.25 mg/kg anti-dkk1-antibody (3:1, $n = 6$), combination of 12.5 mg/kg each of anti-sclerostin- and anti-dkk1-antibody (1:1, $n = 7$), or a combination injection of 6.25 mg/kg of anti-sclerostin-antibody and 18.75 mg/kg of anti-dkk1-antibody (1:3, $n = 7$). (*A*) Loading stiffness, (*B*) unloading stiffness, (*C*) ultimate force, (*D*) energy dissipation, (*E*) displacement, and (*F*) loss tangent of the IVD. Injection groups were compared with the vehicle group using a Dunnett's test, with significance noted below $p < 0.05$.

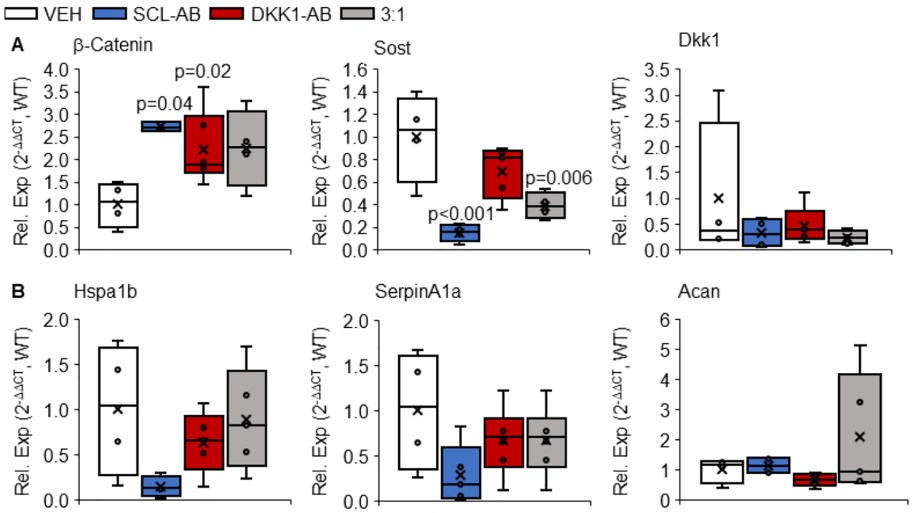

Fig. 3. Injection of scl-Ab and/or dkk1-Ab increased pro-Wnt signaling gene expression. (*A*) Gene expression related to Wnt signaling in tail intervertebral disc (IVD): *β-catenin*, *sost*, and *dkk1*. Gene expression of β-catenin in the 3:1 combination injection was trending toward significance ($p = 0.061$). (*B*) Heat shock protein *hspa1b*, inflammatory marker *serpinA1a*, and extracellular matrix (ECM) marker *aggrecan* expression in the IVD. Scl-Ab injection trended to decrease gene expression of *hspa1b* ($p = 0.069$). Injection groups (veh: $n = 4$; scl-Ab: $n = 5$; dkk1-Ab: $n = 6$; and 3:1: $n = 5$) were compared with the vehicle group using a Dunnett's test, with significance noted below $p < 0.05$.

Statistics

Post ANOVA, a Dunnett's test was used for the injection-related studies, with vehicles as the main comparison. A one-sample *t* test was used to test for outliers beyond 3 SD. A Student's *t* test was used between WT and *sost* KO IVD and between veh and Scl-Ab. Box plots were used as the main graphical output. A box plot displays a five-number summary of the data. The top and bottom lines of the box plot represent the first and third quartile, while the center line in the box is the median. The top and bottom points represent the minimum and maximum of the data. Each point on the graph represents one sample. Total number of samples for each analysis are included in the figure legend. False discovery rate (FDR) was computed from *p* values using the Benjamini-Hochberg procedure. A *p* value or FDR value (where applicable) < 0.05 was considered significant.

Results

Injection of neutralization for sclerostin, dkk1, and in 3:1 combination increased IVD height

Preliminary data suggested that the IVD gene expression of *sost* relative to *dkk1* is ~3:1 (data not shown). Therefore, in addition to scl-Ab or dkk1-Ab, we injected mice at 3:1, 1:1, and 1:3 scl-Ab: dkk1-Ab for consistency. Systemic administration of scl-Ab, dkk1-Ab, and the 3:1 combination of scl-Ab and dkk1-Ab increased lumbar IVD height ($F = 7.74$ and $p < 0.001$) by 22%, 26%, and 32% ($p = 0.02$, 0.02, 0.005), respectively (Fig. 1*A*, *B*) but the 1:1 and 1:3 combination injections did not significantly increase IVD height. Neither IVD degeneration score nor proteoglycan staining intensity were altered by any injections. In tail IVD, no variety of injection impacted IVD height ($F = 0.73$ and $p = 0.60$), proteoglycan staining intensity ($F = 3.88$ and $p = 0.01$), or IVD degeneration score ($F = 1.25$ and $p = 0.31$) (Supplemental Fig. S1).

Injection of sclerostin-neutralization antibody improved IVD mechanics

Despite no change in tail IVD height by injection of any Wnt signaling inhibitor neutralization combination compared with vehicle injection, injection of scl-Ab alone most improved the

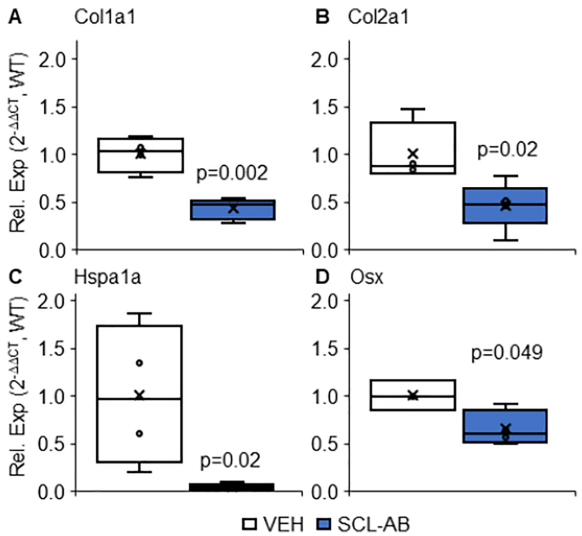

Fig. 4. Scl-Ab injection reduced extracellular matrix (ECM), heat shock protein, and osterix gene expression in the intervertebral disc (IVD). Gene expression of scl-Ab injection ($n = 5$) compared with the vehicle-treated tail IVD ($n = 4$) for (*A*) *cola1a*, (*B*) *col2a1*, (*C*) *hspa1a*, and (*D*) *osx*. Student's *t* tests compared groups, with significance noted below $p < 0.05$.

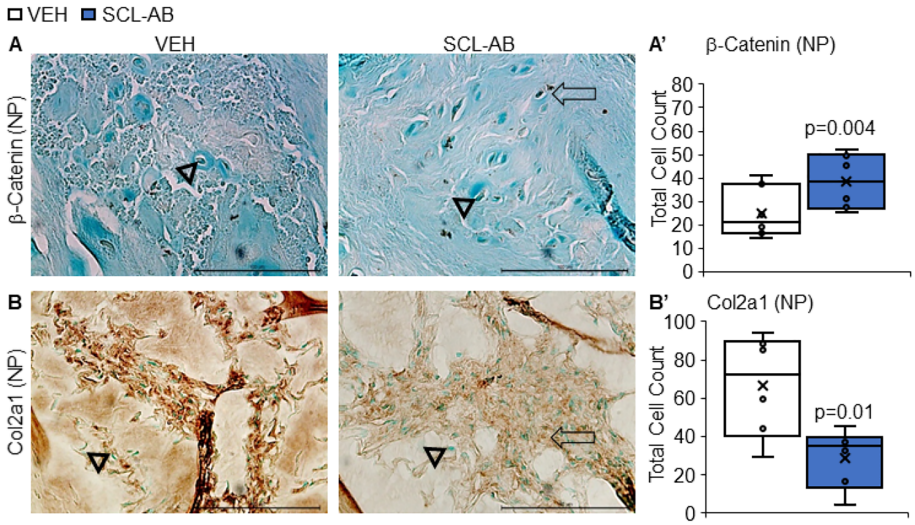

Fig. 5. Scl-Ab injection promoted β-catenin protein expression in the nucleus pulposus (NP). (*A*) Images of β-catenin protein expression in the NP of the tail intervertebral disc (IVD) of vehicle ($n = 7$) and anti-sclerostin antibody group ($n = 6$). (*A'*) Quantitative measurements of the fraction of β-catenin protein-expressing cells to the total number of cells in the NP. (*B*) Images of col2a1 protein expression in the NP of the vehicle ($n = 6$) and sclerostin antibody group ($n = 6$). (*B'*) Quantitative measurements of the fraction of col2a1 protein-expressing cells to the total number of cells in the NP. Scale bar = 100 μm. Student's *t* tests compared groups, with significance noted below $p < 0.05$.

mechanical properties of tail IVD. Namely, injection of scl-Ab doubled ($p = 0.006$, $p = 0.008$, respectively) the loading ($F = 2.52$ and $p = 0.05$) and unloading stiffness ($F = 2.76$ and $p = 0.04$) of the IVD (Fig. 2). A similar trend appeared with ultimate force, but no changes were statistically significant ($F = 1.35$ and $p = 0.27$). Neither energy dissipation, displacement, nor loss tangent was affected by any injection group ($F = 3.44$, 1.62, 1.59, and $p = 0.01$, 0.18, 0.19).

Injection of sclerostin-neutralization-, dkk1-, and 3:1 combinatorial-antibody stimulated Wnt signaling

Quantitative PCR was determined in the injection groups that increased IVD height relative to vehicle: scl-Ab, dkk1-Ab, and 3:1 scl-Ab:dkk1-Ab. Scl-Ab and dkk1-Ab upregulated transcription of canonical Wnt signaling co-factor *β-catenin* ($F = 4.346$ and $p = 0.01$) by 1.7-fold ($p = 0.04$) and 1.2-fold ($p = 0.02$),

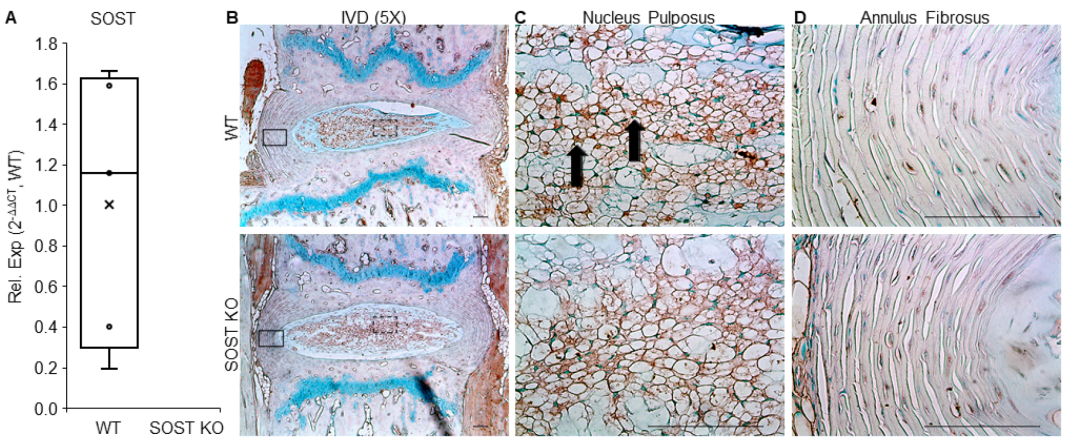

Fig. 6. *Sost* deletion reduced *sost* gene and protein expression in the intervertebral disc (IVD). *Sost* gene expression from qPCR and qualitative images of sclerostin staining of the WT and *sost* KO IVD ($n = 5$) was effectively deleted from the *sost* KO group. (*A*) qPCR of *sost* from WT IVD (CT: 34.09–34.87, 25–75%). *Sost* gene expression was not detected in *sost* KO IVD. (*B*) Magnified images (40×) of the nucleus pulposus (NP) of the WT IVD (top) and *sost* KO IVD (bottom) using Alcian blue counterstain to show sclerostin protein expression in the cells of the IVD. The WT expressed defined dark brown staining (black arrows), whereas the *sost* KO cells expressed less, more diffuse staining, indicating less sclerostin expression in the *sost* KO. (*C*) Magnified image (40×) of the annulus fibrosus (AF). Scale bar = 100 μm. Dashed box represents the highlighted NP portion (*C*). Solid box represents the highlighted portion of the AF (*D*).

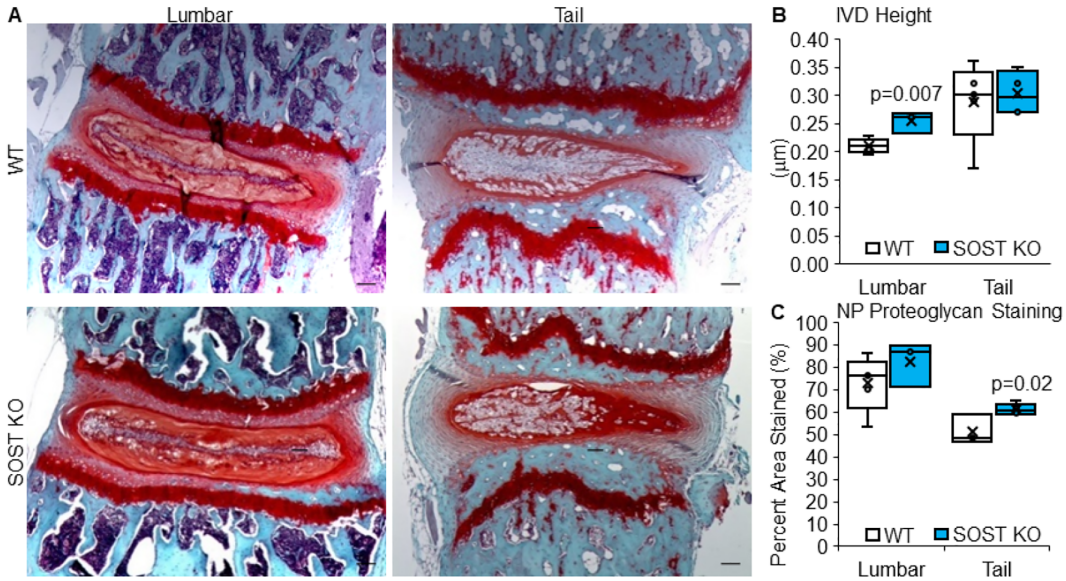

Fig. 7. Deletion of *sost* promoted intervertebral disc (IVD) height and proteoglycan staining. (*A*) Magnified images (5×) of Safranin O and fast green counterstain of lumbar and tail IVD of the WT group (top row) and *sost* KO group (bottom row; $n = 5$/group). Scale bar = 100 μm. (*B*) Quantitative measurement of the intensity of proteoglycan staining in the IVD. Red staining indicated proteoglycan. (*C*) Quantitative measurement of IVD degeneration score for lumbar and tail IVD of the WT and *sost* KO groups. Student's *t* tests compared groups, with significance noted below $p < 0.05$.

respectively (Fig. 3*A*). Injection of the 3:1 combination trended to upregulate *β-catenin* expression. Corroboratively, scl-Ab reduced *sost* gene expression by 85% ($p = 0.0004$) and 3:1 combination reduced *sost* gene expression by 61% ($p = 0.006$ versus veh, $F = 3.452$, $p = 0.023$). Highly variable *dkk1* expression in the vehicle group obfuscated reduction by each injection group. In addition, we determined the potential regulation of *dkk1* by scl-Ab and vice versa because dkk1 and sclerostin share the capacity to bind the first propeller of LRP5/6 or may compensatorily upregulate the other. Neither injection of antibody significantly regulated the transcription of the other antibody's precursor in the IVD. Heat shock protein a1b (*hspa1b*) gene expression in the IVD was not different between groups, but scl-Ab trended to reduce *hspa1b* ($p = 0.069$). *Hspa1b* and *serpinA1a* were similarly regulated by each antibody injection ($R = 0.83$, $p < 0.05$), but neither *hspa1b* ($F = 2.43$ and $p = 0.11$), *serpina1a* ($F = 1.58$ and $p = 0.23$), nor *aggrecan* ($F = 1.70$ and $p = 0.21$) expression were changed by any injection compared with vehicle (Fig. 3*B*). Inflammation-related markers *cxcl9* and *il-1β* were not detected in any IVD.

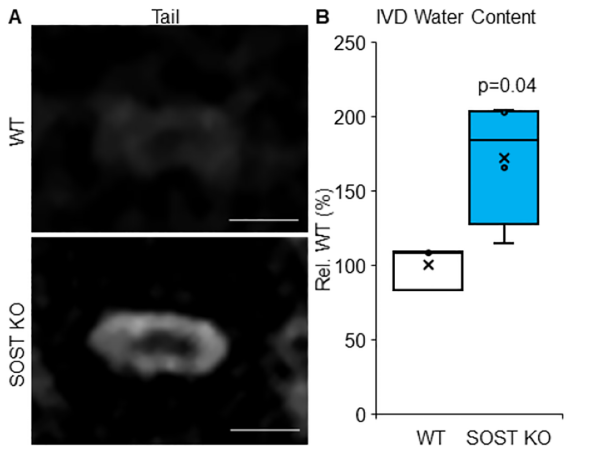

Fig. 8. Deletion of *sost* increased intervertebral disc (IVD) hydration. (*A*) Using a 9.4 T MRI, tail motion segments were imaged, highlighting the IVD of the WT (top; $n = 3$) and *sost* KO (bottom; $n = 4$/group). Scale bar = 1 mm. (*B*) Relative water content was quantified as the area multiplied by intensity, indicating increased hydration in the KO. Student's *t* tests compared groups, with significance noted below $p < 0.05$.

Anti-sclerostin-antibody injection increased *β-catenin* protein and reduced mature NP gene expression in the IVD

Based on the mechanical property improvements by scl-Ab, low variability of upregulation of *β-catenin* by scl-Ab, and trending downregulation of *hspa1b*, we further characterized ECM transcription and cell phenotype in the IVD by scl-Ab. Injection of scl-Ab decreased the gene expression of *col1a1* by 57% ($p = 0.002$), *col2a1* by 54% ($p = 0.02$), and *osterix* by 35% ($p = 0.049$) (Fig. 4A, B, and D). Further, scl-Ab increased the number of cells expressing β-catenin protein in the nucleus pulposus by 81% ($p = 0.004$) and reduced the number of nucleus pulposus cells that expressed *col2a1* by 46% ($p = 0.01$) (Fig. 5B). Similar to *hspa1b*, scl-Ab decreased the gene expression of *hspa1a*, a gene associated with cellular stress,[31] by 95% ($p = 0.02$) (Fig. 5C).

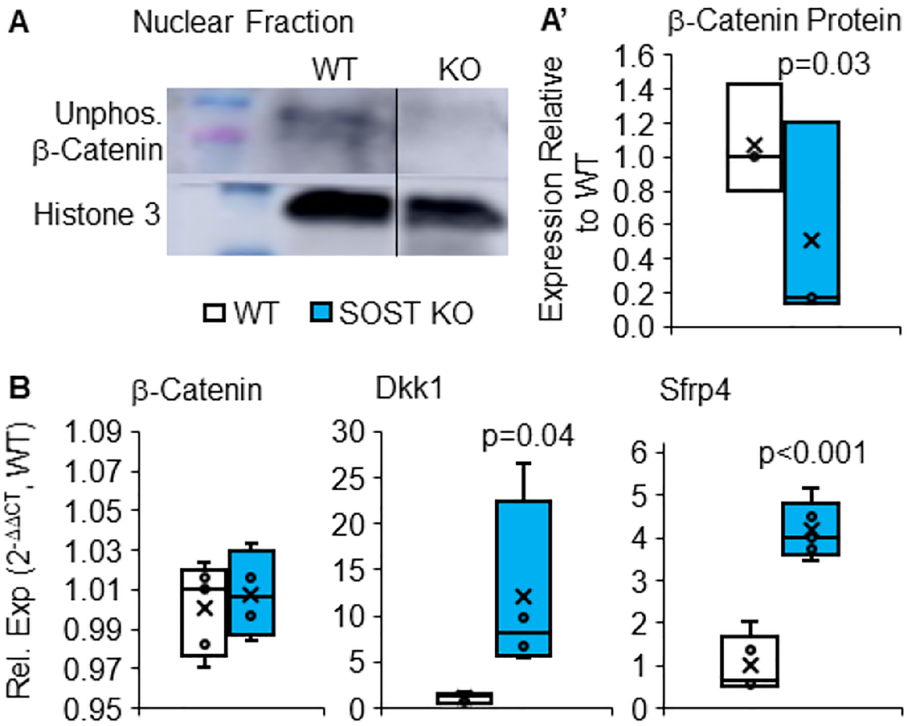

Fig. 9. Deletion of *sost* induced compensation of Wnt signaling by upregulation of Wnt signaling inhibitors. (*A*) Nuclear separation Western blotting (composite image from the same blot) showed a decreased amount of active β-catenin in the cell nuclei of the *sost* KO, using histone 3 as control ($n = 5$/group). (*A'*) Quantitative measurement of β-catenin protein expression from Western blot. Unphosphorylated (active) β-catenin at 92 kDa, histone 3 at 17 kDa, β-Actin at 92 kDa. (*B*) Whereas β-catenin is unchanged, *dkk1* and *sfrp4*, both inhibitors of the pathway, were increased in response to *sost* deletion. Student's *t* tests compared groups, with significance noted below $p < 0.05$.

Systemic deletion of *sost* reduced sclerostin protein expression in the IVD

Quantitatively, *sost* gene expression was consistently detectable in the WT IVD, but *sost* was not detected in any of the *sost* KO IVD (Fig. 6*A*). Qualitatively, sclerostin protein expression (brown staining, black arrow) appeared in the NP cells of WT IVD (Fig. 6*B*). By contrast, sclerostin staining in the *sost* KO was minimally expressed in NP cell nuclei and relegated to the cell membrane and extracellular matrix (Fig. 6*C*). The AF minimally expressed sclerostin (Fig. 6*D*).

Deletion of *sost* in the IVD increased IVD height, proteoglycan staining, and hydration

Proteoglycans are hydrophilic proteins, and loss of proteoglycans is a common feature of IVD degeneration.[32,33] Compared with WT IVD, deletion of *sost* KO increased lumbar IVD height by 21% ($p = 0.007$) and tail proteoglycan staining by 150% ($p = 0.02$) in the NP (Fig. 7*A–C*). However, the accumulation of proteoglycan staining, while potentially beneficial for hydration, led to slight disorganization of the band of cells in the NP, statistically insignificantly increasing the histological IVD degeneration score (Supplemental Fig. S2). Next, we determined the

Table 3. Area, Intensity, and Water Content Determined by MRI in WT and *sost* KO Intervertebral Disc

Genotype	Area (mm^2)	Intensity	Water content
WT 1	0.32	956	301.12
WT 2	0.32	1235	395.20
WT 3	0.32	1004	391.56
WT AVG	**0.34 ± 0.04**	**1065 ± 149**	**362.63 ± 52.29**
SOST KO 1	0.65	1145	739.67
SOST KO 2	0.64	1155	733.43
SOST KO 3	0.34	1225	416.50
SOST KO 4	0.40	1501	600.40
SOST KO AVG	**0.51 ± 0.16**	**1257 ± 167**	**622.50 ± 151.61***

Student's *t* tests compared groups, with significance noted $p < 0.05$ (*). Values in bold represent the mean.

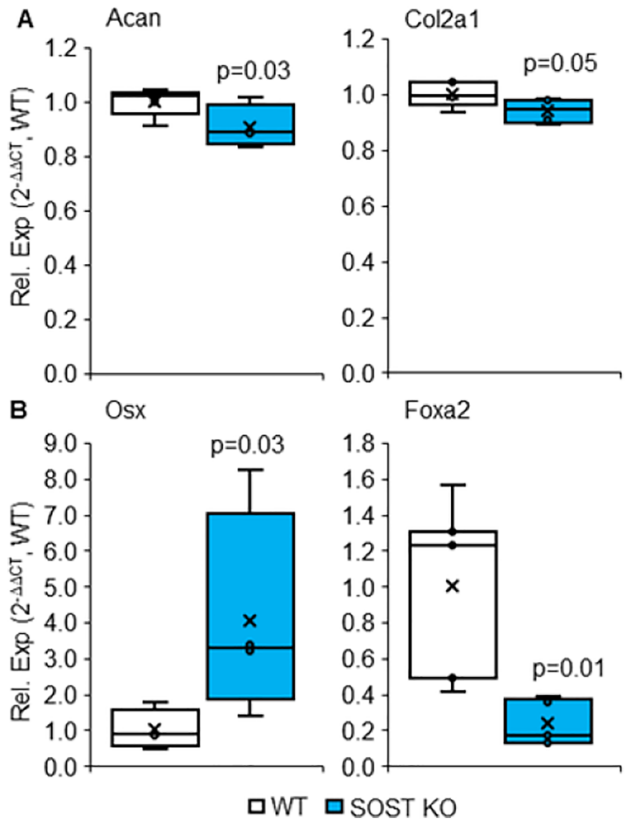

Fig. 10. Global deletion of *sost* induced the gene expression of a mature cell type in the intervertebral disc (IVD). Gene expression of (*A*) extracellular matrix (ECM) and (*B*) transcription factors of cell type markers in WT and *sost* KO IVD ($n = 5$, group). Student's *t* tests compared groups, with significance noted below $p < 0.05$.

hydration of the IVD by MRI, a standard noninvasive clinical imaging technique for determining the morphology and hydration of the IVD.[34,35] WT IVD had patched distribution of water, while the ring of water that demarcated the cell band from the AF was clearer and brighter in the *sost* KO IVD (Fig. 8). Relative to the WT IVD, *sost* KO increased the estimated water content, ie, hydration, by 72% ($p = 0.04$), but there was no statistical difference in the total area of the IVD or intensity of the water between groups (Fig. 8; Table 3 rpinA1d, sostdc1, keratin8, wnt16). These data show that deletion of *sost* imbibed the IVD.

Sost deletion induced compensatory normalization of Wnt signaling by upregulation of Wnt signaling inhibitors

Canonical Wnt signaling requires translocation of β-catenin to the cell nucleus. Therefore, we determined the nuclear and cytoplasmic fraction of β-catenin protein. *Sost* KO IVD had less active β-catenin protein in the cell nuclei than WT IVD (Fig. 9*A*), suggesting *less* Wnt signaling. The cytoplasmic fraction was not statistically different between groups (Supplemental Fig. S3). In addition, dkk1 is a target of Wnt/β-catenin signaling, so we also determined the gene expression of Wnt inhibitors. Sost KO IVD expressed greater *dkk1* by 10-fold ($p = 0.04$) and *sfrp4* by four-fold ($p < 0.001$, Fig. 9*B*). Lack of difference in gene expression of co-transcription factor *β-catenin* between WT and sost KO IVD suggested compensation of Wnt signaling after deletion of *sost*.

Table 4. Genes Not Significantly Regulated by *sost* Deletion or Expressed in the Intervertebral Disc

Gene	WT	*Sost* KO	*p* Value
SerpinA1C+	1 ± 0.18	0.72 ± 0.09	0.06
SerpinA1D	1 ± 0.56	0.52 ± 0.19	0.11
Sostdc1	1 ± 0.35	1.86 ± 0.71	0.11
Keratin8	1 ± 0.83	0.50 ± 0.50	0.26
Wnt 16	1 ± 0.69	1.79 ± 1.46	0.36
Axin 2	1 ± 0.53	1.38 ± 0.75	0.38
SerpinA1A	1 ± 0.37	0.52 ± 0.19	0.80
Cxcl9	Undetermined	Undetermined	N/A
IL-1β	Undetermined	Undetermined	N/A
Wnt 3a	Undetermined	Undetermined	N/A

N/A = not applicable. Student's *t* tests compared groups, with significance noted $p < 0.05$.

Compensation of Wnt signaling from *sost* deletion triggered extracellular matrix degradation and the expression of a mature NP cell phenotype in the IVD

Sost KO regulated gene and protein expression of extracellular matrix metabolism toward anti-anabolism, catabolism, and IVD cell phenotypes toward chondrogenesis. Specifically, deletion of *sost* downregulated gene expression of *aggrecan* by 52% ($p = 0.03$) (Fig. 10*A*). Common markers of notochordal cells and mature NP cells were determined, respectively. *Sost* KO IVDs expressed less transcription of notochordal marker *foxA2*[36] by 77% ($p = 0.01$) (Fig. 10*B*), less transcription of early NP marker *col2a1* by 67% ($p = 0.05$) (Fig. 10*A*), and fewer cells in the NP-expressed *col2a1* (Fig. 11*A*, *A*′). By contrast, accrual of mature NP can be marked by increased chondrogenic marker[37] and osteoblast transcription factor sp7 (Osx). Compared to WT IVD, *sost* KO IVD expressed increased osterix gene expression by 4.4-fold ($p = 0.03$) and protein expression (Figs. 10*B* and 11*B*, *B*′). Sost deletion similarly altered gene expression in lumbar IVD from rna-seq with upregulation of ECM degradation, downregulation of notochordal marker *gdf5*,[38] downregulation of early mature NP markers (*ColX*[39]), and upregulation of mature NP cell marker *bglap* (Supplemental Fig. S4). Gene expression that was not statistically different between WT and *sost* KO IVD included *serpinA1a-c* (*serpinA1c+*, $p = 0.06$), *serpinA1d*, *sostdc1*, *keratin8*, *wnt16*, Water Content Determined by *axin2*, *serpinA1a*, *cxcl9*, *il-1β*, and *wnt3a* (Table 4).

Using whole transcriptomic analysis, *sost* deletion downregulated pathways related to protein folding and upregulated pathways related to immune response in the IVD

In an overall sense, based on the PCA plot (Fig. 12*A*), *sost* KO IVDs are not transcriptomically distinct from WT IVDs. Nevertheless, 35% of the top 20 downregulated pathways were related to cellular response to external stimuli (e.g., protein folding, FDR < 0.05), 15% to metabolism, 15% to extracellular matrix organization, 10% to gene expression, and 5% to developmental biology, signaling transduction, metabolism of proteins, transportation of small molecules, and other pathways (Fig. 12*B*), whereas of the top 20 upregulated pathways, 85% were related

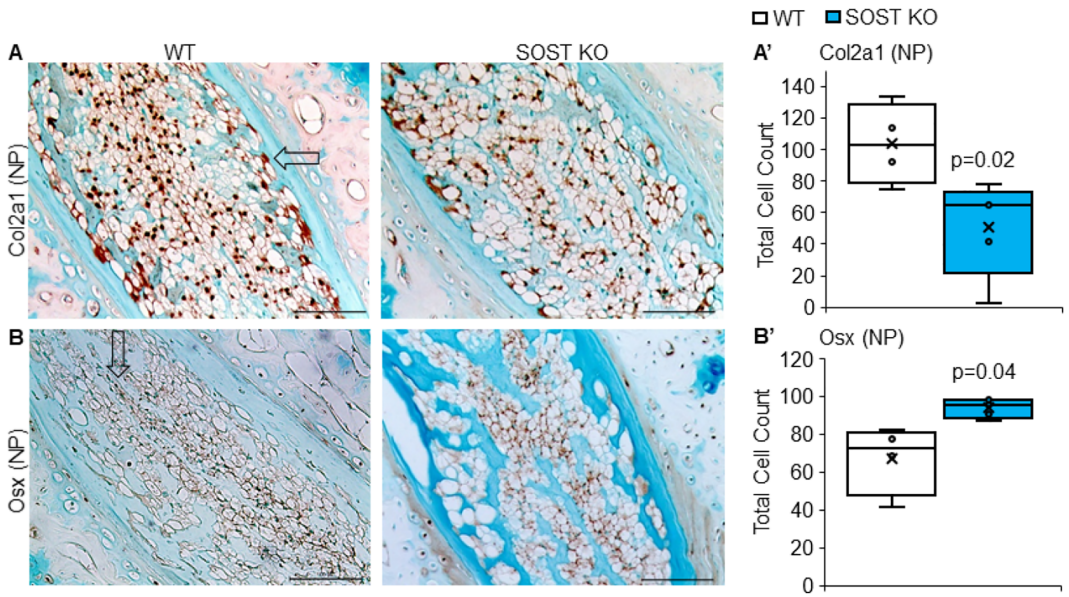

Fig. 11. Global deletion of *sost* induced the protein expression of a mature nucleus pulposus (NP) cell phenotype. (*A*) Collagen 2 staining and (*B*) osterix staining of the NP of the WT and *sost* KO ($n = 5$/group). Quantitative measurement of the fraction of the number of positively (brown) stained (arrow) (*A'*) collagen 2-expressing cells and (*B'*) osterix-expressing cells. Student's *t* tests compared groups, with significance noted below $p < 0.05$.

to immune pathways (FDR < 0.05) and 5% each to cell cycle (FDR < 0.05), signaling transduction (FDR < 0.05), and hemostasis (FDR < 0.05). Specifically, the heat map for the top downregulated pathway was "protein folding," which included heat shock proteins, and for the top upregulated pathway was immune response (Fig. 12*C*). More specifically, the volcano plot highlights in red the genes that were most significantly differentially regulated (Fig. 12*D*). A list of the top 20 differentially downregulated and top 20 upregulated were included (Tables 5 and 6). Lastly, GSEA analysis for the *sost* KO IVDs corroborated that Wnt signaling was reduced based on the normalized enrichment score (−1.53, FDR < 0.01; Tables 7 and 8; Supplemental Fig. S5).

Sost KO and scl-Ab increased vertebral bone structure

Osteocytes and osteoblasts are the predominate sclerostin-expressing cells.[13,40] Here, WT tail vertebra expressed sclerostin staining in both osteocytes and osteoblasts, whereas global deletion of *sost* blunted its expression in the vertebra (Supplemental Fig. S6) and, consequently, increased trabecular and cortical bone structure (Table 8). Scl-Ab may have induced a compensatory upregulation of sclerostin protein (Supplemental Fig. S7). Separately, scl-Ab increased the number of osteocytes expressing substance P because of the need for innervation during bone formation.[41]

Discussion

FDA-approved anti-sclerostin antibody (scl-Ab) augmented the structure and strength of the IVD. We hypothesized that increasing Wnt signaling by suppression of Wnt competitors by pharmacological or genetic approaches would augment the structure of the IVD. Sclerostin and dkk1 are known inhibitors of the canonical Wnt signaling pathway and work in a similar fashion.[42] Scl-Ab, dkk1-Ab, and the 3:1 combinatorial injection of sclerostin and dkk1 increased lumbar IVD height via strong upregulation of Wnt/β-catenin signaling, but injection of a 1:1 ratio of sclerostin to dkk1 antibody or a 1:3 ratio were not as beneficial. By contrast, only scl-Ab injection improved the mechanical properties of the IVD. Prolonged suppression of sclerostin by global deletion of *sost* increased IVD height, water content, and proteoglycan staining but induced a significant normalization of Wnt signaling. Overall, these data show that systemic administration of scl-Ab promotes major features of the IVD that are lost with IVD degeneration.

Sclerosteosis patients with a *sost* gene mutation are associated with greater bone mass and stature.[43] Although mice with injection of scl-Ab,[44] conditional deletion of sost in bone cells, or global KO of *sost* all have greater bone mass, vertebral bone length does not change.[45] Therefore, neutralization of *sost*/sclerostin may extend IVD height by direct stimulation of Wnt signaling and/or adaptation to greater bone mass.

IVD cells express Wnt signaling inhibitors *sost*/sclerostin and dkk1,[11] but their role in the IVD was undetermined. Nucleus pulposus-specific upregulation and downregulation of Wnt signaling co-transcription factor β-catenin is anabolic and catabolic to the ECM/stiffness of the IVD, respectively.[12] Here, injections of scl-Ab, dkk1-Ab, and in combination increased IVD height and β-catenin gene expression. We also administered combinatorial injections of scl-Ab and dkk1-Ab (3:1, 1:1, and 1:3), where 3:1 injection outperformed 1:1 and 1:3 injections in increasing IVD height. Therefore, we excluded 1:1 and 1:3 injections from further examination. The 3:1 injection most closely approximated the WT gene expression of sost relative to dkk1, which could have most effectively neutralized sclerostin and dkk1 to upregulate Wnt/β-catenin signaling in the IVD.

Our data and others have noted that sclerostin and dkk1 share a mutual compensatory regulation of the Wnt/β-catenin signaling pathway,[11,12,20] which may impact IVD cell differentiation. We found that global sost deletion induced a strong

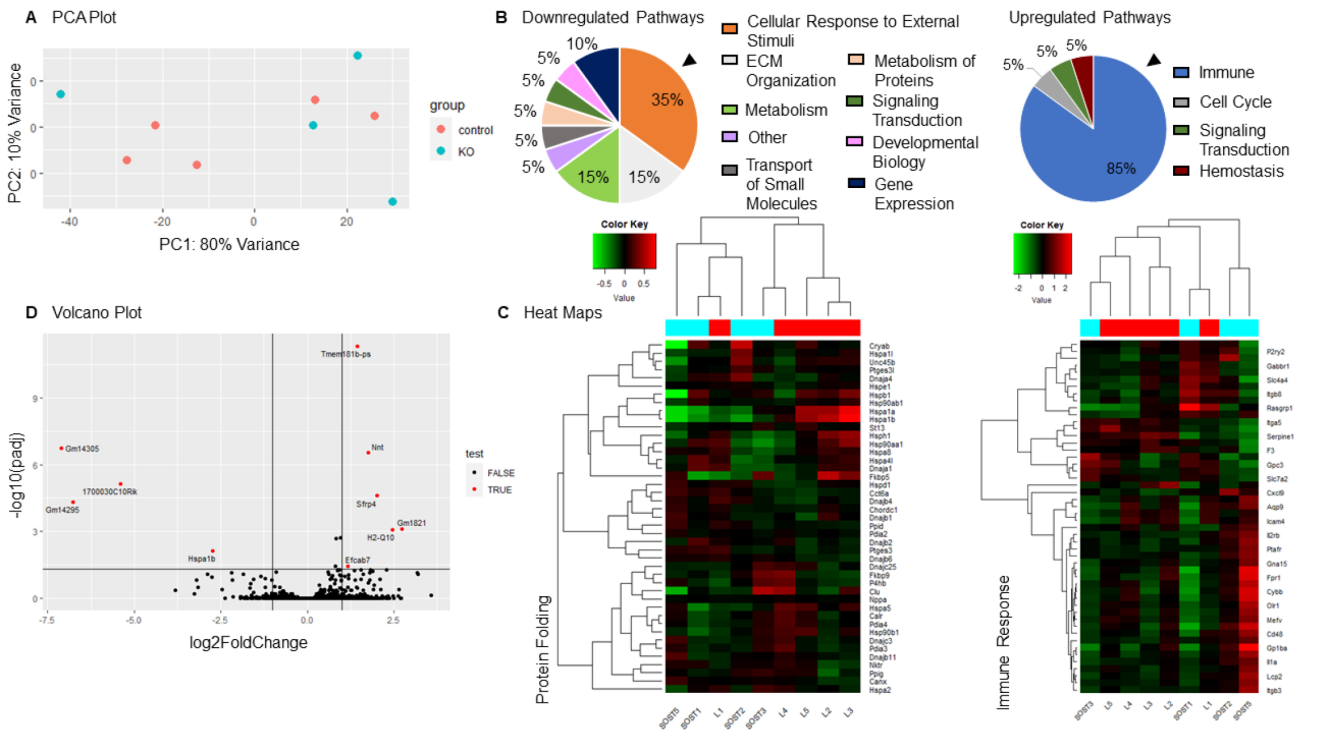

Fig. 12. RNA sequencing of *sost* KO and WT intervertebral disc (IVD). (*A*) PCA plot of *sost* KO ($n = 4$) and WT ($n = 5$) IVDs demonstrating an overlap between the groups. (*B*) Top 20 downregulated and top 20 upregulated pathways after *sost* deletion. (*C*) Corresponding heat maps for protein folding associated with the top downregulated pathway (arrowhead in *B*) and immune response associated with the top upregulated pathway (arrowhead in *B*). (*D*) Volcano plot of all differentially regulated genes, with labels of most significantly regulated genes (FDR < 0.05).

upregulation of Wnt signaling inhibitors that consequently normalized β-catenin protein in IVD cell nuclei and Wnt signaling. Normalization of Wnt signaling may have attenuated the initial benefits of activation and could explain the subdued difference between *sost* KO and WT IVD. Similarly, we noted compensation of sclerostin in osteocytes of sclerostin-antibody-treated mice. Next, we previously found that similar to ECM anabolism,[12] regulation of Wnt signaling in the IVD was associated with differential regulation of cell type expression

Table 5. Top 20 Genes Upregulated by *Sost* KO

Gene	Fold change	*p* Value	False discovery rate
Ntn	3.34	<0.001	<0.001
Tmem181b-ps	2.66	<0.001	<0.001
Sfrp4	3.97	<0.001	<0.001
Gm1821	6.58	<0.001	0.002
H2-Q10	5.36	<0.001	0.007
Wdfy1	1.90	<0.001	0.091
Mepe	3.66	<0.001	0.149
Clec10a	3.49	<0.001	0.233
Sp6	2.85	<0.001	0.268
Cd1d1	2.53	<0.001	0.340
Fasn	2.91	<0.001	0.340
Tnfrsf19	1.79	<0.001	0.359
Scd1	3.43	<0.001	0.364
Dgat2	2.27	<0.001	0.364
Serping1	1.93	<0.001	0.371
Agppat2	1.94	<0.001	0.421
Cxcl9	3.35	0.001	0.512
Cebpa	1.95	0.001	0.513
Efcab7	2.21	0.001	0.513
Myh7	33.95	0.001	0.513

Table 6. Top 20 Genes Downregulated by *Sost* KO

Gene	Fold change	*p* Value	False discovery rate
Gm14305	−109.99	<0.001	<0.001
1700030C10Rik	−153.71	<0.001	<0.001
Hspa1b	−37.64	<0.001	<0.001
Hist1h1b	−6.72	<0.001	0.051
Hsph1	−7.38	<0.001	0.254
Rec8	−2.34	<0.001	0.286
Eps8l1	−8.73	<0.001	0.286
Rn45s	−3.69	<0.001	0.286
Hspa1a	−4.57	<0.001	0.286
Aldh3a1	−4.52	0.001	0.513
Serpine1	−2.97	0.001	0.513
Slc15a2	−3.13	0.001	0.513
Nfatc2	−9.53	0.002	0.565
Erdr1	−1.93	0.002	0.656
Foxa2	−3.21	0.002	0.656
Gm7120	−2.34	0.003	0.656
Egr1	−2.08	0.003	0.776
Hsp90aa1	−1.75	0.003	0.788
Gdf5	−1.96	0.005	1.000

Table 7. Top 20 Downregulated Pathways by *Sost* Deletion

Name	Normalized enrichment score	Nominal *p* value	False discovery rate
Interferon α-response	−1.57	<0.001	0.007
Bile acid metabolism	−1.56	<0.001	0.006
Notch signaling	−1.56	0.010	0.006
Wnt β-catenin signaling	−1.53	0.011	0.008
Peroxisome	−1.52	0.001	0.009
Allograft rejection	−1.51	0.001	0.010
Interferon γ-response	−1.47	0.000	0.016
UV response DN	−1.39	0.006	0.036
Xenobiotic metabolism	−1.36	0.006	0.047
Fatty acid metabolism	−1.32	0.013	0.072
Kras signaling up	−1.30	0.006	0.082
Adipogenesis	−1.29	0.004	0.089
Coagulation	−1.26	0.059	0.118
IL6 JAK STAT3 signaling	−1.23	0.112	0.161
Inflammatory response	−1.16	0.133	0.317
Angiogenesis	−1.15	0.263	0.311
Hedgehog signaling	−1.11	0.326	0.441
Oxidative phosphorylation	−1.09	0.226	0.479
Apical junction	−1.09	0.243	0.478
Complement	−1.09	0.262	0.462

(notochordal cell, e.g., brachyury, versus mature NP cell, e.g., osterix). Conditional stabilization of β-catenin in nucleus pulposus cells using a Shh-CreERT2 driver promotes brachyury and reduces osterix, whereas deletion of β-catenin using the Shh-CreERT2 driver reduces brachyury and promotes osterix. Similarly, here, stimulation of Wnt signaling by scl-Ab promoted β-catenin and reduced osterix, but Wnt signaling compensation after *sost* deletion reduced notochordal markers (*krt19*, *foxa2*,[46] and *gdf5*[38]) and increased mature NP cell markers (osterix[21] and bglap). Therefore, persistent suppression of sclerostin may need to be avoided to limit potential compensatory cell differentiation in healthy IVD, and it is unclear if this compensation would occur in degenerated IVD.

IVD degeneration is characterized by a loss of IVD height from proteoglycan breakdown and dehydration,[47,48] which is necessary for the IVD to withstand spinal mechanical forces and function properly. Although many of the combinations tested here similarly upregulated β-catenin gene expression and IVD height, scl-Ab injection alone most functionally strengthened the IVD. In corroboration, deletion of *sost* increased the proteoglycan staining in the nucleus pulposus and increased water content, as measured by MRI. These data suggest that regulation of sclerostin may have additional downstream effects from canonical Wnt signaling that impact the material mechanical properties of the IVD.

Although sclerostin and dkk1 are both inhibitors of canonical Wnt signaling, sclerostin and dkk1 can inhibit different Wnt ligands[42] and impose distinct regulation of targets. Our data suggest that they may distinctly regulate heat shock protein (Hsp) expression and other genes related to protein folding. Cross-talk between Hsps and Wnt signaling has been previously proposed to mediate axial patterning and cell proliferation, where long-term induction of Hsps reduces Wnt targets brachyury, TCF, and Wnt3.[49] In the IVD, Hsps are responsive to environmental stresses[31] and are differentially regulated by mechanical strain.[47] For instance, loss of mechanical signals by cellular disanchoring reduces *hsp* gene expression and compressive mechanical strains upregulate *hsp* gene expression in nucleus pulposus cells.[50] *Hspa1a* and *hspa1b* are both expressed in the IVD,[51] and although scl-Ab and dkk1-Ab induced similar upregulation of β-catenin, only scl-Ab downregulated *hsps*. Similarly, *sost* deletion reduced *hsps*, even though Wnt signaling was normalized in these IVDs. These data suggest that neutralization of sclerostin reduces *hsps*, rather than by activation of Wnt signaling itself.

We would like to address some of the limitations of the study. First, scl-Ab is prescribed to postmenopausal women, and although we injected female mice, our KO mice were males. Nevertheless, we expect similar effects of *sost* deletion in female IVD.[8,20] Future experiments will include determining the effect of anti-sclerostin injections to counter challenges to the disc, eg, aging and injury, and the ability of systemic injection of anti-sclerostin to reach the IVD. Second, qPCR was performed on entire IVDs and the effect of *sost* KO could not be differentiated by gene expression, but key outcomes were further discerned in a localized manner using immunohistochemistry. Although we did not note any histological protein changes of β-catenin nor sclerostin in the annulus fibrosus by regulation of sost/sclerostin, a more localized approach may discern these potential changes. Further, proteoglycan content estimation by histology will require corroboration. Third, silencing Wnt signaling in IVD cells induces ECM degradation[20,52] but also promotes anti-inflammation.[53] By contrast, activating Wnt signaling in murine IVD leads to elevated ECM production[54] but also promotes pro-inflammatory signals.[53] Based on ECM metabolism, our data suggest that Wnt signaling was increased by anti-Wnt signaling inhibitor injection and sost deletion (at least initially), but *sost* deletion also induced upregulation of immune pathways. Injection of scl-Ab did not upregulate immune-related genes; therefore, the pulsatile upregulation of Wnt signaling by scl-Ab as occurs clinically may preclude the consequences of an inflammatory response. Despite these limitations, we show that upregulation of Wnt signaling by persistent and long-term absence of *sost* hydrates the IVD and promotes ECM expression in lumbar IVD, but compensation of Wnt signaling may induce mild mature cell differentiation.

In conclusion and in addition to the well-recognized attributes to bone structure, suppression of *sost*/sclerostin or dkk1 augmented IVD structure. Combinatorial injection of scl-Ab and

Table 8. *Sost* KO Vertebral Bone Structural Properties

	Tail		Lumbar	
Bone parameter	WT	*Sost* KO	WT	*Sost* KO
Tb.BV/TV (%)	49.4 ± 3.1	53.5 ± 4.6	25.3% ± 4.8	45.7 ± 5.1*
Tb.N (1/mm)	5.52 ± 0.30	5.84 ± 0.14	6.11 ± 0.50	6.45 ± 0.76
Tb.Th (mm)	0.09 ± 0.01	0.09 ± 0.01	0.07 ± 0.01	0.07 ± 0.01

Tb.BV/TV = trabecular bone volume; Tb.N = trabecular number; Tb.Th = trabecular thickness. *: $p < 0.05$

dkk1-Ab similarly increased IVD height as each alone, when the ratio of the administration reflected in vivo ratios, but scl-Ab alone most strengthened the IVD. Persistent genetic deletion of *sost* increased proteoglycan staining and IVD hydration but also induced a compensatory upregulation of Wnt signaling inhibitors that consequently normalized Wnt signaling. Together, these data show that the musculoskeletal benefits of scl-Ab romosozumab (Evenity), which is commercially available, may extend beyond bone to improve key features of the IVD and could potentially be used as a therapeutic for IVD degeneration.

Disclosures

All authors state that they have no conflicts of interest.

Acknowledgments

Funding was provided by Biomedical Research Grant (EC), Biomechanics and Biomaterials Research Center grant (NH), Start-up (NH), and ORS Spine Section Travel Fellowship (NB). We thank the Indiana Center for Musculoskeletal Health (ICMH) for their support. In addition, we thank Washington University in St. Louis for access to the Structure and Strength Core. Authors' roles: TK: data curation; formal analysis; methodology; writing–original draft; writing–review and editing. NB: data curation; formal analysis; writing–original draft. PJN: formal analysis; writing–original draft. DFE: formal analysis. ELC: data curation; formal analysis; methodology; writing–original draft; writing–review and editing. AGR: methodology; resources; writing–original draft; writing–review and editing. NH: conceptualization; formal analysis; funding acquisition; investigation; methodology; project administration; resources; supervision; validation; writing–original draft; writing–review and editing.

Author Contributions

Tori Kroon: Data curation; formal analysis; methodology; writing – original draft; writing – review and editing. **Neharika Bhadouria:** Data curation; formal analysis; writing – original draft. **Paul Niziolek:** Formal analysis; writing – original draft. **Daniel Edwards III:** Formal analysis. Roy Choi: Data curation; **Erica L Clinkenbeard:** Data curation; formal analysis; methodology; writing – original draft; writing – review and editing. **Alexander Robling:** Methodology; resources; writing – original draft; writing – review and editing. **Nilsson Holguin:** Conceptualization; formal analysis; funding acquisition; investigation; methodology; project administration; resources; supervision; validation; writing – original draft; writing – review and editing.

Peer Review

The peer review history for this article is available at https://publons.com/publon/10.1002/jbmr.4546.

Data Availability Statement

The data that support the findings of this study are openly available in biorixiv at http://doi.org/10.1101/2021.07.01.449486 (2021), reference number [2021.2007.2001.449486]

References

1. Basso M, Cavagnaro L, Zanirato A, et al. What is the clinical evidence on regenerative medicine in intervertebral disc degeneration? Musculoskelet Surg. 2017;101:93-104. https://doi.org/10.1007/s12306-017-0462-3.
2. Loibl M, Wuertz-Kozak K, Vadala G, Lang S, Fairbank J, Urban JP. Controversies in regenerative medicine: Should intervertebral disc degeneration be treated with mesenchymal stem cells? JOR Spine. 2019;2. https://doi.org/10.1002/jsp2.1043.
3. Papavassiliou AG, Pneumaticos SG, Evangelopoulos DS. Biologic treatment of mild and moderate intervertebral disc degeneration. Mol Med Published online. 2014;20:400-409. https://doi.org/10.2119/molmed.2014.00145.
4. Dowdell J, Erwin M, Choma T, Vaccaro A, Iatridis J, Cho SK. Intervertebral disk degeneration and repair. Clin Neurosurg. 2017;8:3S. https://doi.org/10.1093/neuros/nyw078.
5. Livshits G, Ermakov S, Popham M, et al. Evidence that bone mineral density plays a role in degenerative disc disease: the UK twin spine study. Ann Rheum Dis. 2010;69(12):2102-2106. https://doi.org/10.1136/ard.2010.131441.
6. Cosman F, Crittenden DB, Adachi JD, et al. Romosozumab treatment in postmenopausal women with osteoporosis. N Engl J Med. 2016;375(16):1532-1543. https://doi.org/10.1056/NEJMoa1607948.
7. FDA approves new treatment for osteoporosis in postmenopausal women at high risk of fracture. Case Med Res. 2019. doi:https://doi.org/10.31525/fda2-ucm635653.htm
8. Li X, Ominsky MS, Niu QT, et al. Targeted deletion of the sclerostin gene in mice results in increased bone formation and bone strength. J Bone Miner Res. 2008;23(6):860-869. https://doi.org/10.1359/jbmr.080216.
9. Holguin N, Brodt MD, Silva MJ. Activation of Wnt signaling by mechanical loading is impaired in the bone of old mice. J Bone Miner Res. 2016;31(12):2215-2226. https://doi.org/10.1002/jbmr.2900.
10. van Bezooijen RL, Roelen BAJ, Visser A, et al. Sclerostin is an osteocyte-expressed negative regulator of bone formation, but not a classical BMP antagonist. J Exp Med. 2004;199(6):805-814. https://doi.org/10.1084/jem.20031454.
11. Witcher PC, Miner SE, Horan DJ, et al. Sclerostin neutralization unleashes the osteoanabolic effects of Dkk1 inhibition. JCI Insight. 2018;3(11):e98673. https://doi.org/10.1172/jci.insight.98673.
12. Holguin N, Silva MJ. In-vivo nucleus Pulposus-specific regulation of adult murine intervertebral disc degeneration via Wnt/Beta-catenin signaling. Sci Rep 2018;8:11191. https://doi.org/10.1038/s41598-018-29352-3.
13. Holdsworth G, Roberts SJ, Ke HZ. Novel actions of sclerostin on bone. J Mol Endocrinol. 2019;62(2):R167-R185. https://doi.org/10.1530/JME-18-0176.
14. Lojk J, Marc J. Roles of non-canonical Wnt signalling pathways in bone biology. Int J Mol Sci. 2021;22(19):10840. https://doi.org/10.3390/ijms221910840.
15. Zhu M, Tang D, Wu Q, et al. Activation of β-catenin signaling in articular chondrocytes leads to osteoarthritis-like phenotype in adult β-catenin conditional activation mice. J Bone Miner Res. 2009;24(1):12-21. https://doi.org/10.1359/jbmr.080901.
16. Bourhis E, Tam C, Franke Y, et al. Reconstitution of a Frizzled8·Wnt3a·LRP6 signaling complex reveals multiple Wnt and Dkk1 binding sites on LRP6. J Biol Chem. 2010;285(12):9172-9179. https://doi.org/10.1074/jbc.M109.092130.
17. van Dinther M, Zhang J, Weidauer SE, et al. Anti-Sclerostin antibody inhibits internalization of Sclerostin and Sclerostin-mediated antagonism of Wnt/LRP6 signaling. PLoS One. 2013. https://doi.org/10.1371/journal.pone.0062295.
18. Ettenberg SA, Charlat O, Daley MP, et al. Inhibition of tumorigenesis driven by different Wnt proteins requires blockade of distinct ligand-binding regions by LRP6 antibodies. Proc Natl Acad Sci USA. 2010;107(35):15473-15478. https://doi.org/10.1073/pnas.1007428107.

19. Niida A, Hiroko T, Kasai M, et al. DKK1, a negative regulator of Wnt signaling, is a target of the beta-catenin/TCF pathway. Oncogene. 2004; 23(52):8520-8526. https://doi.org/10.1038/sj.onc.1207892.

20. Kondo N, Yuasa T, Shimono K, et al. Intervertebral disc development is regulated by wnt/β-catenin signaling. Spine. 2011;36(8):E513-E518. https://doi.org/10.1097/BRS.0b013e3181f52cb5.

21. Silva MJ, Holguin N. Aging aggravates intervertebral disc degeneration by regulating transcription factors toward chondrogenesis. FASEB J. 2020;34(2):1970-1982. https://doi.org/10.1096/fj.201902109R.

22. Holguin N, Aguilar R, Harland RA, Bomar BA, Silva MJ. The aging mouse partially models the aging human spine: lumbar and coccygeal disc height, composition, mechanical properties, and Wnt signaling in young and old mice. J Appl Physiol. 2014;116(12):1551-1560. https://doi.org/10.1152/japplphysiol.01322.2013.

23. Smolders LA, Meij BP, Riemers FM, et al. Canonical Wnt signaling in the notochordal cell is upregulated in early intervertebral disk degeneration. J Orthop Res. 2012;30(6):950-957. https://doi.org/10.1002/jor.22000.

24. Cappello R, Bird JLE, Pfeiffer D, Bayliss MT, Dudhia J. Notochordal cell produce and assemble extracellular matrix in a distinct manner, which may be responsible for the maintenance of healthy nucleus pulposus. Spine. 2006;31(8):873-882. https://doi.org/10.1097/01.brs.0000209302.00820.fd.

25. Li X, Ominsky MS, Warmington KS, et al. Sclerostin antibody treatment increases bone formation, bone mass, and bone strength in a rat model of postmenopausal osteoporosis. J Bone Miner Res. 2009; 24(4):578-88. https://doi.org/10.1359/jbmr.081206.

26. Diarra D, Stolina M, Polzer K, et al. Dickkopf-1 is a master regulator of joint remodeling. Nat Med. 2007;13(2):156-163. https://doi.org/10.1038/nm1538.

27. Tam V, Chan WCW, Leung VYL, et al. Histological and reference system for the analysis of mouse intervertebral disc. J Orthop Res. 2018;36(1):233-243. https://doi.org/10.1002/jor.23637.

28. Liu JW, Abraham AC, Tang SY. The high-throughput phenotyping of the viscoelastic behavior of whole mouse intervertebral discs using a novel method of dynamic mechanical testing. J Biomech. 2015; 48(10):2189-2194. https://doi.org/10.1016/j.jbiomech.2015.04.040.

29. Holguin N, Brodt MD, Sanchez ME, Silva MJ. Aging diminishes lamellar and woven bone formation induced by tibial compression in adult C57BL/6. Bone. 2014;65:83-91. https://doi.org/10.1016/j.bone.2014.05.006.

30. Clinkenbeard EL, Farrow EG, Summers LJ, et al. Neonatal iron deficiency causes abnormal phosphate metabolism by elevating FGF23 in normal and ADHR mice. J Bone Miner Res. 2014;29(2):361-369. https://doi.org/10.1002/jbmr.2049.

31. Chooi WH, Chan SCW, Gantenbein B, Chan BP. Loading-induced heat-shock response in bovine intervertebral disc organ culture. PLoS One. 2016;11(11):e0167406. https://doi.org/10.1371/journal.pone.0161615.

32. Kiani C, Chen L, Wu YJ, Yee AJ, Yang BB. Structure and function of aggrecan. Cell Res. 2002;12:19-32. https://doi.org/10.1038/sj.cr.7290106.

33. Wei Q, Zhang X, Zhou C, Ren Q, Zhang Y. Roles of large aggregating proteoglycans in human intervertebral disc degeneration. Connect Tissue Res. 2019;2021:9954909. Published 2021 Jul 28. https://doi.org/10.1080/03008207.2018.1499731.

34. Marinelli NL, Haughton VM, Muñoz A, Anderson PA. T 2 relaxation times of intervertebral disc tissue correlated with water content and proteoglycan content. Spine. 2009;34(5):520-4. https://doi.org/10.1097/BRS.0b013e318195dd44.

35. Grunert P, Hudson KD, Macielak MR, et al. Assessment of intervertebral disc degeneration based on quantitative magnetic resonance imaging analysis: An in vivo study. Spine. 2014;39(6):E369-78. https://doi.org/10.1097/BRS.0000000000000194.

36. Zhou X, Ma C, Hu B, et al. FoxA2 regulates the type II collagen–induced nucleus pulposus–like differentiation of adipose-derived stem cells by activation of the Shh signaling pathway. FASEB J. Published online. 2018. https://doi.org/10.1096/fj.201800373R.

37. Minogue BM, Richardson SM, Zeef LAH, Freemont AJ, Hoyland JA. Transcriptional profiling of bovine intervertebral disc cells: Implications for identification of normal and degenerate human intervertebral disc cell phenotypes. Arthritis Res Ther. 2010;12(1):R22. https://doi.org/10.1186/ar2929.

38. Hodgkinson T, Shen B, Diwan A, Hoyland JA, Richardson SM. Therapeutic potential of growth differentiation factors in the treatment of degenerative disc diseases. JOR Spine. 2019;2(1):e1045. https://doi.org/10.1002/jsp2.1045.

39. Aigner T, Greskötter KR, Fairbank JCT, von der Mark K, Urban JPG. Variation with age in the pattern of type X collagen expression in normal and scoliotic human intervertebral discs. Calcif Tissue Int. 1998;63(3): 263-268. https://doi.org/10.1007/s002239900524.

40. Weivoda MM, Youssef SJ, Oursler MJ. Sclerostin expression and functions beyond the osteocyte. Bone. 2017;96:45-50. https://doi.org/10.1016/j.bone.2016.11.024.

41. Tomlinson RE, Christiansen BA, Giannone AA, Genetos DC. The role of nerves in skeletal development, adaptation, and aging. Front Endocrinol. 2020;11:646. https://doi.org/10.3389/fendo.2020.00646.

42. Ke HZ, Richards WG, Li X, Ominsky MS. Sclerostin and dickkopf-1 as therapeutic targets in bone diseases. Endocr Rev Published online. 2012;33:747-783. https://doi.org/10.1210/er.2011-1060.

43. Beighton P, Durr L, Hamersma H. The clinical features of sclerosteosis. A review of the manifestations in twenty five affected individuals. Ann Intern Med. 1976;84(4):393-397. https://doi.org/10.7326/0003-4819-84-4-393.

44. Cardinal M, Chretien A, Roels T, et al. Gender-related impact of Sclerostin antibody on bone in the osteogenesis imperfecta mouse. Front Genet. 2021;12:705505. https://doi.org/10.3389/fgene.2021.705505.

45. Yee CS, Manilay JO, Chang JC, et al. Conditional deletion of Sost in MSC-derived lineages identifies specific cell-type contributions to bone mass and B-cell development. J Bone Miner Res. 2018;33(10): 1748-1759. https://doi.org/10.1002/jbmr.3467.

46. Maier JA, Lo YT, Harfe BD. Foxa1 and Foxa2 are required for formation of the intervertebral discs. PLoS. One. 2013. https://doi.org/10.1371/journal.pone.0055528.

47. Bowles RD, Setton LA. Biomaterials for intervertebral disc regeneration and repair. Biomaterials Published online. 2017;129:54-67. https://doi.org/10.1016/j.biomaterials.2017.03.013.

48. Vo NV, Hartman RA, Patil PR, et al. Molecular mechanisms of biological aging in intervertebral discs. J Orthop Res. 2016;34(8):1289-306. https://doi.org/10.1002/jor.23195.

49. Duffy DJ, Millane RC, Frank U. A heat shock protein and Wnt signaling crosstalk during axial patterning and stem cell proliferation. Dev Biol. 2012;362:271–281. https://doi.org/10.1016/j.ydbio.2011.11.014.

50. Chooi WH, Chan BP. Compression loading-induced stress responses in intervertebral disc cells encapsulated in 3D collagen constructs. Sci Rep. 2016;6:26449. https://doi.org/10.1038/srep26449.

51. Takao T, Iwaki T. A comparative study of localization of heat shock protein 27 and heat shock protein 72 in the developmental and degenerative intervertebral discs. Spine. 2002;27:361–367. https://doi.org/10.1097/00007632-200202150-00007.

52. Mundy C, Yasuda T, Kinumatsu T, et al. Synovial joint formation requires local Ext1 expression and heparan sulfate production in developing mouse embryo limbs and spine. Dev Biol. 2011;351(1): 70-81. https://doi.org/10.1016/j.ydbio.2010.12.022.

53. Hiyama A, Yokoyama K, Nukaga T, Sakai D, Mochida J. A complex interaction between Wnt signaling and TNF-α in nucleus pulposus cells. Arthritis Res Ther. 2013. https://doi.org/10.1186/ar4379.

54. Winkler T, Mahoney EJ, Sinner D, Wylie CC, Dahia CL. Wnt signaling activates Shh signaling in early postnatal intervertebral discs, and re-activates Shh signaling in old discs in the mouse. PLoS One. Published online. 2014. https://doi.org/10.1371/journal.pone.0098444.[a]